IOP Publishing Physica Scripta
Phys. Scr. **95** (2020) 044001 (11pp) https://doi.org/10.1088/1402-4896/ab5735

Structural inpainting techniques using equations of engineering physics

Tudor Barbu

Institute of Computer Science, Romanian Academy—Iaşi Branch, Iaşi, Romania

E-mail: tudor.barbu@iit.academiaromana-is.ro

Received 29 July 2019, revised 23 October 2019
Accepted for publication 13 November 2019
Published 11 February 2020

Abstract

A comprehensive survey on structure-based inpainting methods based on equations of engineering physics is provided in this work. Diffusion equations, describing the random motion of the micro-particles in physics, have been successfully applied in the image processing areas in the last decades. Nonlinear anisotropic diffusion-based structural inpainting techniques, using variational and non-variational PDE models, are discussed first. Influential variational interpolation approaches, such as those using the Mumford–Shah functional, total variation inpainting and its versions, and Euler's Elastica inpainting, are addressed here. Second and fourth-order anisotropic diffusion-based interpolation schemes, some of them not following variational principles, are then presented. Our own contributions in this field are also discussed. The applications of the reaction-diffusion equations, like Ginzburg–Landau equation, describing a large variety of physics phenomena, in the inpainting domain, are described next. Structural reconstructions methods using partial differential equations for fluid dynamics, such as the Navier–Stokes equations describing the motion of the viscous fluids, are then considered here. Other state of the art third-order PDE-based structural inpainting algorithms surveyed here are based on the curvature-driven diffusion equations that use the thermal diffusion principle in physics. Fourth-order PDE-based interpolation solutions, such as Cahn–Hilliard inpainting that uses a modified mathematical physics equation describing the phase separation process, are also described.

Keywords: image interpolation, anisotropic diffusion models, reaction-diffusion equations, curvature driven diffusion-based inpainting, equations of fluid dynamics for inpainting, Cahn–Hilliard inpainting

(Some figures may appear in colour only in the online journal)

1. Introduction

Partial differential equations (PDE) have long been used to construct mathematical models in the physics of continuous media [1]. Because these differential equations express continuous change, they have been used to model dynamical phenomena in heat conduction, fluid mechanics, elasticity, vibrating strings, electromagnetism and many other physics and engineering areas.

Also, the equations of engineering physics have been successfully applied in the image processing domain in the last 35 years. The origin of the PDEs is physics, since these equations are closely related to the world governed by physical laws, but they have been intensively applied to various sub-domains of image processing and analysis, too [1].

Since the equations that describe the natural phenomena hold for a continuum and the images can be analyzed in continuous spaces, these PDEs have been successfully used to develop some effective image restoration, interpolation, segmentation, compression, registration, decomposition and motion estimation solutions in the last decades, which solve properly the challenges that still exist in these fields. They offer some important advantages to these domains, such as their rigorous mathematical foundation, their modeling flexibility and their fast and accurate numerical approximation methods.

In this paper we focus on the PDEs of physics applied in the image interpolation domain. The aim of the image interpolation, known also as *inpainting* or *completion*, is to recover the missing or highly damaged image regions using the information of the known surrounding areas of the image [2].

The inpainting domain has some important application areas, such as digital artwork reconstruction, undesired object and text removal, image compression and image zooming and super-resolution. The inpainting approaches may have a texture-based, structure-based or combined character. The textural inpainting techniques, which can be based on texture synthesis [3] or represent exemplar-based techniques [4], do not represent the focus of our research. Only the structural inpainting is considered here.

The structural inpainting techniques employ information around the missing regions to estimate the isophotes from coarse to fine, and diffuse that information by a diffusion mechanism. The main motivation of choosing the PDEs for image reconstruction is that the PDE-based interpolation models perform automatically an effective inpainting of the missing regions while not altering the known part. They avoid the unintended effects, like blurring, thus preserving properly the essential image features, such as the edges and corners. The state of the art structure-based interpolation methods using PDEs of engineering physics is surveyed here.

So, the inpainting techniques based on nonlinear diffusion equations are described in the next section. While some of them follow variational principles, other have a non-variational character.

Then, the image interpolation based on the reaction-diffusion equations is addressed in the third section. Structural inpainting solutions using third-order PDEs for fluid dynamics are presented in the fourth section, while the curvature-driven diffusion (CDD)-based inpainting is described in the fifth section. The sixth section is dedicated to the image reconstruction approaches based on nonlinear fourth-order PDEs for physics. The article ends with a section of conclusions and a list of references.

2. Nonlinear diffusion-based image interpolation

The diffusion represents the process in physics that is related to moving from an area of high concentration to a zone of low concentration. This physical process equilibrates the concentration differences and conserves the mass, since it does only transports it, without creating or destroying the mass.

Diffusion equations represent PDEs that describe this behavior of the collective motion of micro-particles in a material that results from the random movement of each particle, in physics [5]. These equations are obtained from the Fick's laws of diffusion, which describe the diffusion process [5]. Thus, they have the general form $\frac{\partial u}{\partial t} = \mathrm{div}(D \cdot \nabla u)$, where D represents the diffusivity and u is the concentration.

These equations are useful in numerous domains, including image processing, where the concentration is identified to the grayscale value at a given location and the diffusion coefficient D may take various forms depending on the image processing task. In this section we discuss the application of the nonlinear diffusion equations to the image interpolation field.

While some PDE-based inpainting models follow variational principles, being derived from minimization problems, other diffusion schemes cannot be expressed as variational models, being directly provided as evolutionary differential equations. Some state of the art variational image interpolation techniques are surveyed in the next subsection, while some nonlinear diffusion-based inpainting solutions are described in PDE form in the second subsection.

2.1. Variational models for structure-based inpainting

The energy-based structural inpainting algorithms recover the image affected by missing regions by minimizing energy cost functionals of the form:

$$\min_u \left(J(u) = R(u) + \frac{1}{2}\int_\Omega \lambda_\Gamma (u - u_0)^2 \mathrm{d}\Omega \right), \tag{1}$$

where the image domain $\Omega \subseteq R^2$, Γ is the inpainting region, the inpainting mask is given by $\lambda_\Gamma = \lambda \cdot 1_{\Omega\setminus\Gamma}$, $\lambda > 0$, the regularizing term $R(u)$ containing a-priori information from the image u is responsible for the filling process, and the fidelity term $\frac{1}{2}\int_\Omega \lambda_\Gamma (u - u_0)^2 \mathrm{d}\Omega$ makes the minimizer to remain close enough to the observed image u_0 outside of the inpainting domain [6]. The corresponding diffusion equation-based model is achieved from (1) by using the Euler–Lagrange equation and the gradient descent method [7].

Many variational inpainting solutions have been obtained by considering various versions of the regularizer term. Thus, the harmonic inpainting model is characterized by $R(u) = \int_\Omega \|\nabla u\|^2 \mathrm{d}x\mathrm{d}y$ [2]. It represents a quite simple interpolation approach that does not satisfy properly the connectivity principle.

Other early variational reconstruction approaches are based on the Mumford–Shah image segmentation model. One of them uses the Γ-convergence approximation of the Mumford–Shah functional [8], being given by the next minimization:

$$\min_u \left(\frac{1}{2}\int_\Omega \lambda_\Gamma (u - u_0)^2 \mathrm{d}\Omega + \frac{\gamma}{2}\int_{\Omega\setminus\Gamma} z_\epsilon^2 \, |\nabla u|^2 \mathrm{d}\Omega + \alpha \int_\Omega \left(\epsilon |\nabla z_\epsilon|^2 + \frac{(1 - z_\epsilon)^2}{4\epsilon} \right) \mathrm{d}\Omega \right), \tag{2}$$

where z_ϵ denotes the signature function of the edge set [8]. This inpainting technique is characterized by a low complexity and a fast numerical convergence, and preserves the image details very well.

Total variation (TV) inpainting developed by Chan and Shen [9], which constitutes a very influential variational

interpolation model, is described by the minimization:

$$\min_{u\in L^2(\Omega)}\left(E[u]=\int_\Omega \alpha\|\nabla u\|\ \mathrm{d}x\mathrm{d}y+\frac{\lambda_\Gamma}{2}\int_\Omega (u-u_0)^2\mathrm{d}x\mathrm{d}y\right). \tag{3}$$

It inpaints successfully the missing regions by minimizing the first-order TV while keeping close to the initial image in the known part. Also, it achieves a good connectivity, but not for very large image gaps, and may generate the undesired staircase effect. The following nonlinear second-order anisotropic diffusion model is obtained from TV inpainting scheme, by applying the Euler–Lagrange equation and then the steepest gradient descent method [7]:

$$\begin{cases}\frac{\partial u}{\partial t}=\alpha\nabla\cdot\left(\frac{\nabla u}{|\nabla u|}\right)-\lambda_\Gamma(u-u_0)\\ u(0,x,y)=u_0\end{cases}.$$

Many TV-based reconstruction approaches of higher orders that improve the TV inpainting technique have been developed. So, the TV^2 inpainting model is obtained by considering the second-order TV as regularizer function: $R(u)=\int_\Omega|\nabla^2 u|\ \mathrm{d}x\mathrm{d}y$ [2]. It outperforms TV inpainting, obtaining a better interpolation and more natural reconstructed images, and overcomes better the staircasing. TV^2 inpainting represents also a better connectivity solution, providing a proper interpolation along large gaps.

Some variational techniques combine the first and the second order TV regularizations to achieve improved inpainting results. Such a TV + TV^2 inpainting model [10] is based on the following minimization:

$$u^*=\arg\min_u\left(\frac{\lambda_\Gamma}{2}\int_{\Omega\setminus\Gamma}(u-u_0)^2\mathrm{d}x\mathrm{d}y+\int_\Omega\alpha(x)|\nabla u|\ \mathrm{d}x\mathrm{d}y+\int_\Omega\beta(x)|\nabla^2 u|\ \mathrm{d}x\mathrm{d}y\right), \tag{4}$$

where $\alpha(x)$ and $\beta(x)$ represent two properly modeled spatially varying functions.

This compound variational inpainting solution provides effective completion results, outperforming both TV and TV^2 inpainting schemes. It interpolates succesfully large missing zones and avoids the unintended effects. It is numerically solved by applying the Split Bregman algorithm [10].

Other improved TV-based inpainting frameworks are the total generalized variation inpainting [11], Blind inpainting using l_0 and TV regularization [12] and TV inpainting with primal-dual active set method [13].

Another influential higher-order variational inpainting technique is Euler's Elastica inpainting model, developed by Chan and Shen [14]. It is derived from (1) by considering the regularizer:

$$R(u)=\int_\Gamma w(u)\left(\alpha+\beta\left(\nabla\cdot\frac{\nabla u}{|\nabla u|}\right)^2\right)|\nabla u|\ \mathrm{d}x\mathrm{d}y, \tag{5}$$

where the coefficients $\alpha,\beta>0$ control the behavior of this scheme and $w(u)$ is a weighting function depending on the evolving image's histogram. This approach is able to inpaint large missing regions and works properly in noisy conditions, also. Euler's Elastica inpainting provides a much better connectivity than TV inpainting model, being able to interpolate successfully along much larger gaps [14].

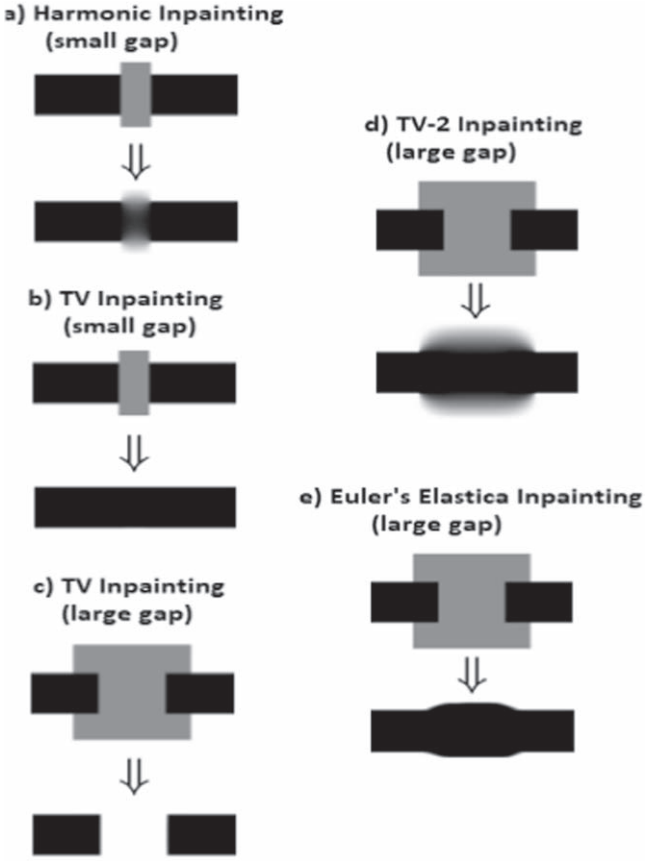

Figure 1. Reconstruction results achieved by various inpainting models.

The connectivity power of the described variational inpainting techniques is illustrated in figure 1.

We have also developed numerous energy-based structural inpainting techniques and disseminated them in our past works. While some of them are mainly based on various forms of the regularizer component in (1) [15], other variational interpolation solutions proposed by us have a hybrid character, combining some nonlinear second and fourth order diffusions [16].

2.2. Nonlinear second-order PDE-based inpainting

In the previous subsection we have described nonlinear diffusion-based inpainting models that follow the variational principle and are expressed in energy-based form. Other diffusion-based structural inpainting techniques are provided in a second-order PDE-based form, many of them not following variational principles and directly given as evolutionary PDEs.

Since image denoising and inpainting represent closely related fields, the PDE-based interpolation models can be derived from the PDE restoration schemes by applying some inpainting masks to them. Besides the PDE form of TV

inpainting described in the previous subsection, which can be derived from TV Denoising, many other nonlinear diffusion-based interpolation schemes can be obtained from the diffusion-based filtering models [17].

The general form of a nonlinear second-order PDE inpainting model derived from an energy-based scheme is:

$$\frac{\partial u}{\partial t} + \nabla R(u) + \lambda_\Gamma(u - u_0) = 0 \text{ in } \Omega, \tag{6}$$

where $\nabla R(u)$ represents the Frechet derivative of the regularizer function. Depending on the selection of this regularizing component, various second-order PDE-based inpainting techniques have been elaborated in the last decades. We have also developed some second-order anisotropic diffusion-based image interpolation techniques [18].

Non-variational PDE inpainting solutions have been also proposed by us. Their non-variational character is given by the fact that their PDEs cannot be obtained from the minimization of any energy functional [7]. Some of them are based on nonlinear second-order hyperbolic PDE models [19], like the following one:

$$\begin{cases} \gamma\frac{\partial^2 u}{\partial t^2} + \lambda^2\frac{\partial u}{\partial t} - \text{div}(\xi_u(|\nabla u|)\cdot\nabla u) \\ +\beta(1 - 1_M)(u - u_0) = 0 \\ u(0, x, y) = u_0(x, y) \\ \frac{\partial u}{\partial t}(0, x, y) = u_1(x, y) \\ u(t, x, y) = 0, \forall (x, y) \in \partial\Omega\backslash M \end{cases}, \tag{7}$$

where $\gamma, \lambda, \beta \in (0, 1]$, $\xi_u(s) = \varepsilon\left(\frac{K(u)}{\alpha \log_{10}(s + K(u))^k + \nu}\right)^{1/3}$, $\alpha, \varepsilon \in (0, 1)$, $\nu \in (1, 5]$, $k \in \{1, 2, 3, 4\}$ and the conductance parameter $K(u(x, y, t)) = |\eta\text{median}(\nabla u) - \delta t|$, where $\eta \in (1, 3)$ and $\delta \in (0, 1)$. So, the diffusivity function has been constructed as positive, monotonic decreasing and converging to 0, in order to provide a proper image diffusion.

This hyperbolic PDE model is solved numerically by applying a consistent finite difference-based approximation scheme that is proposed in [19]. After performing some computations involving central differences [19], we finally get the next explicit numerical approximation algorithm:

$$u_{i,j}^{n+1} = u_{i,j}^n\left(\frac{4\gamma - 2\beta(1 - 1_M)}{2\gamma + \lambda^2}\right) + u_{i,j}^{n-1}\left(\frac{\lambda^2 - 2\gamma}{2\gamma + \lambda^2}\right) - \\ + \zeta\sum_{q\in N_p}\xi_u(\|\nabla^{p,q}u\|)\cdot\nabla^{p,q}u + u_{i,j}^0\beta(1 - 1_M) = 0 \tag{8}$$

where $n = 0, \ldots, N$, $\nabla^{p,q}u(n) = u(q, n) - u(p, n)$ is the gradient magnitude in a particular direction, N_p is the four-neighborhood of pixel $p = (i, j)$ and $\zeta \in (0, 0.5)$.

It inpaints successfully the missing part, performing well in both clean and noisy conditions, as one can see in figure 2, which describes a noisy image inpainted by various techniques. Method comparison have been also performed. The proposed scheme produces better structural interpolation results than some well-known PDE inpainting schemes, as resulting from table 1, which registers the average PSNR values.

Another non-variational PDE-based inpainting framework developed by us is based on a complex nonlinear second-order anisotropic diffusion model [20], having the next form:

$$\begin{cases} \frac{\partial u}{\partial t} - \psi^u(\|\nabla u\|)\nabla\cdot(\varphi_u(\|\nabla u\|)\nabla u) \\ +\lambda(1 - 1_\Gamma)(u - u_0) = 0, \forall (x, y) \in \Omega \\ u(x, y, 0) = u_0(x, y), \forall (x, y) \in \Omega \\ u(t, x, y) = 0, \forall (x, y) \in \partial\Omega \end{cases}, \tag{9}$$

where $\lambda \in (0, 1]$, the positive and monotonic decreasing diffusivity function $\varphi_u(s) = \delta\left(\frac{\eta(u)}{\xi s^k + \nu\log 10(\eta(u))}\right)^{\frac{1}{k+1}}$, where $\delta \in (0, 2)$, $\xi \in (1, 5]$, $\nu \in (0, 1)$, $k \in \{1, 2, 3, 4\}$ and the conductance parameter $\eta(u(x, y, t)) = |\varepsilon\mu(\|\nabla u\|) + \zeta t|$, where $\varepsilon > 1$ and $\zeta \in (0, 1)$.

The other function used by this model is ψ: $(0, \infty) \to (0, \infty)$, $\psi^u(s) = \gamma(\alpha s^r + \beta)^{\frac{1}{r+1}}$, where $\alpha, \gamma \in (0, 3]$, $\beta \in (0, 3.5]$ and $r \in (0, 2]$. The component based on it, $\psi^u(\nabla u)$, has been introduced to control the speed of the diffusion process.

The following explicit iterative finite difference-based numerical approximation algorithm has been constructed for this anisotropic diffusion model [20]:

$$u_{i,j}^{n+1} = u_{i,j}^n\left(\begin{array}{c} 1 - \lambda(1 - 1_\Gamma) + \\ \psi_{i,j}(\varphi_{i+\frac{1}{2},j} + \varphi_{i-\frac{1}{2},j} + \varphi_{i,j+\frac{1}{2}} + \varphi_{i,j-\frac{1}{2}}) \end{array}\right) \\ + u_{i+1,j}^n\psi_{i,j}\varphi_{i+\frac{1}{2},j} + u_{i-1,j}^n\psi_{i,j}\varphi_{i-\frac{1}{2},j} + u_{i,j+1}^n\psi_{i,j}\varphi_{i,j+\frac{1}{2}} \\ + u_{i,j-1}^n\psi_{i,j}\varphi_{i,j-\frac{1}{2}} + u_{i,j}^0\lambda(1 - 1_\Gamma), \tag{10}$$

where $i \in \{0, 1, \ldots, I\}, j \in \{0, 1, \ldots, J\}, n \in \{0, 1, \ldots, N\}$ and $\varphi_{i\pm\frac{h}{2},j} = \frac{\varphi_{i\pm h,j} + \varphi_{i,j}}{2}$, $\varphi_{i,j\pm\frac{h}{2}} = \frac{\varphi_{i,j\pm h} + \varphi_{i,j}}{2}$.

This algorithm has been successfully used in our inpainting experiments that prove the effectiveness of our nonlinear diffusion technique. It reconstructs properly the damaged images by directing, and also controlling, the speedy diffusion process to the inpainting domain while preserving the details [20].

Also, the proposed approach outperforms other PDE-based interpolation algorithms, by achieving better inpainting results and executing much faster [20]. As one can see in the method comparison example displayed in figure 3, our anisotropic diffusion-based algorithm inpaints completely the deteriorated image in 45 iterations, while other techniques, like TV inpainting, need much more steps for this task.

3. Reaction diffusion-based inpainting solutions

The reaction-diffusion equations represent PDEs that are widely used to describe the pattern formation phenomena in a variety of biological, chemical and physical systems [21]. Since the most common physical phenomena is the change in space and time of the concentration of one or more chemical substances, are naturally applied in the chemistry domain, but the reaction diffusion equations can also describe dynamical

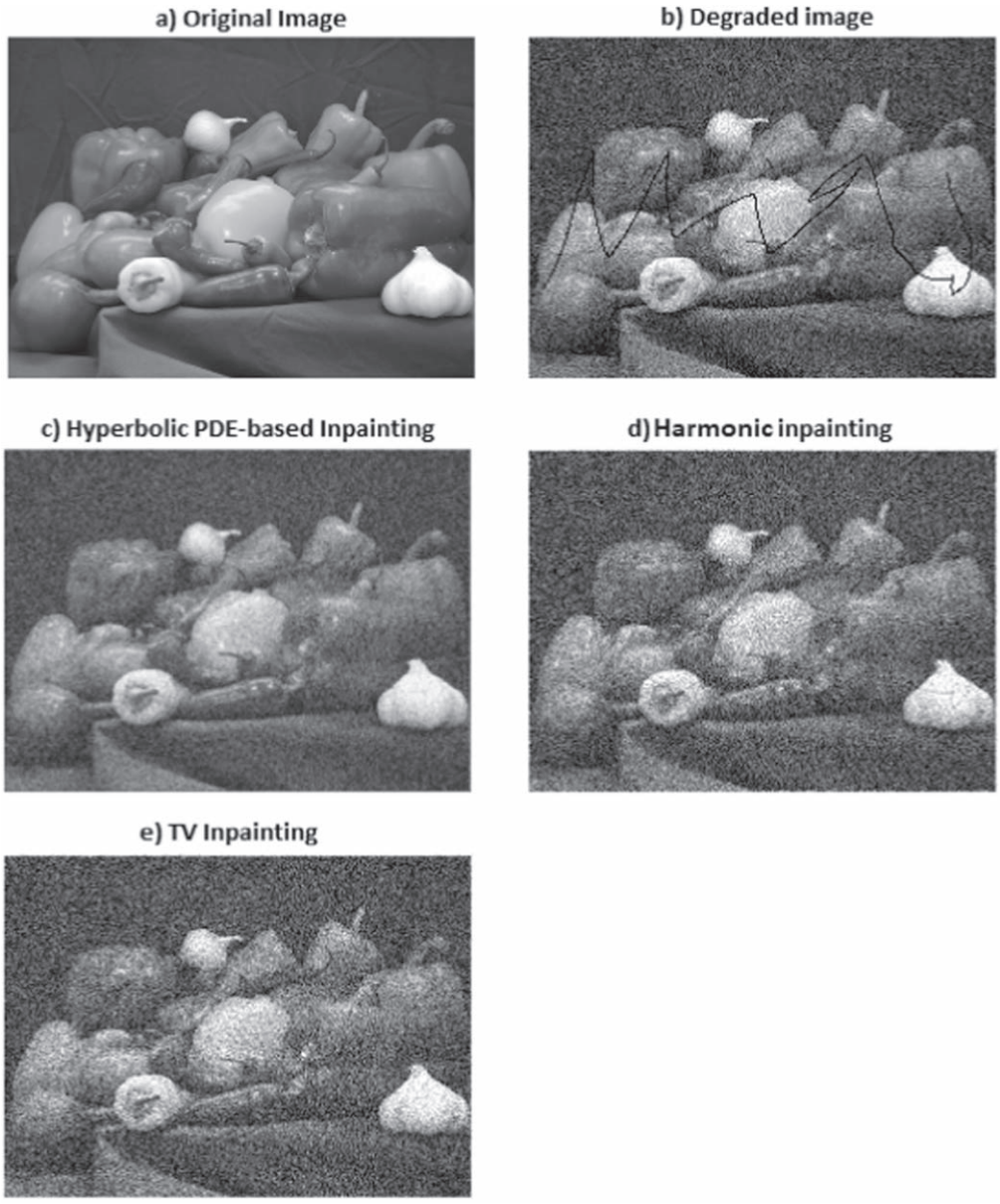

Figure 2. Deteriorated *Peppers* image inpainted by various models.

Table 1. Average PSNR values of several inpainting approaches.

Inpainting algorithm	Average PSNR
This hyperbolic PDE model	31.27 (dB)
TV inpainting	29.86 (dB)
Harmonic inpainting	28.42 (dB)

processes of non-chemical nature, such as the neutron diffusion in physics.

A reaction-diffusion equation is composed of a diffusion component and a reaction term, having the following general form:

$$\frac{\partial u}{\partial t} = D \cdot \Delta u + R(u), \tag{11}$$

where D represents the diffusion coefficient matrix and the function R accounts for all local reactions.

The reaction-diffusion models have been used successfully in the image processing fields in the last years. Thus, effective image restoration has been achieved by applying reaction diffusion-based models that rely on learning [22]. Trained reaction-diffusion models, like those developed by Yu *et al* [23] and based on structural similarity measure, have been successfully used in image interpolation, too.

The solutions of the reaction–diffusion equations display a wide range of behaviors, such as the traveling wave behaviour, which can be described by the complex Ginzburg–Landau equation (CGLE) [24]. A reaction-diffusion system can be described by CGLE when it is close to the onset of the Hopf bifurcation.

The CGLE has been applied successfully in the inpainting domain [24]. First, the interpolation algorithm,

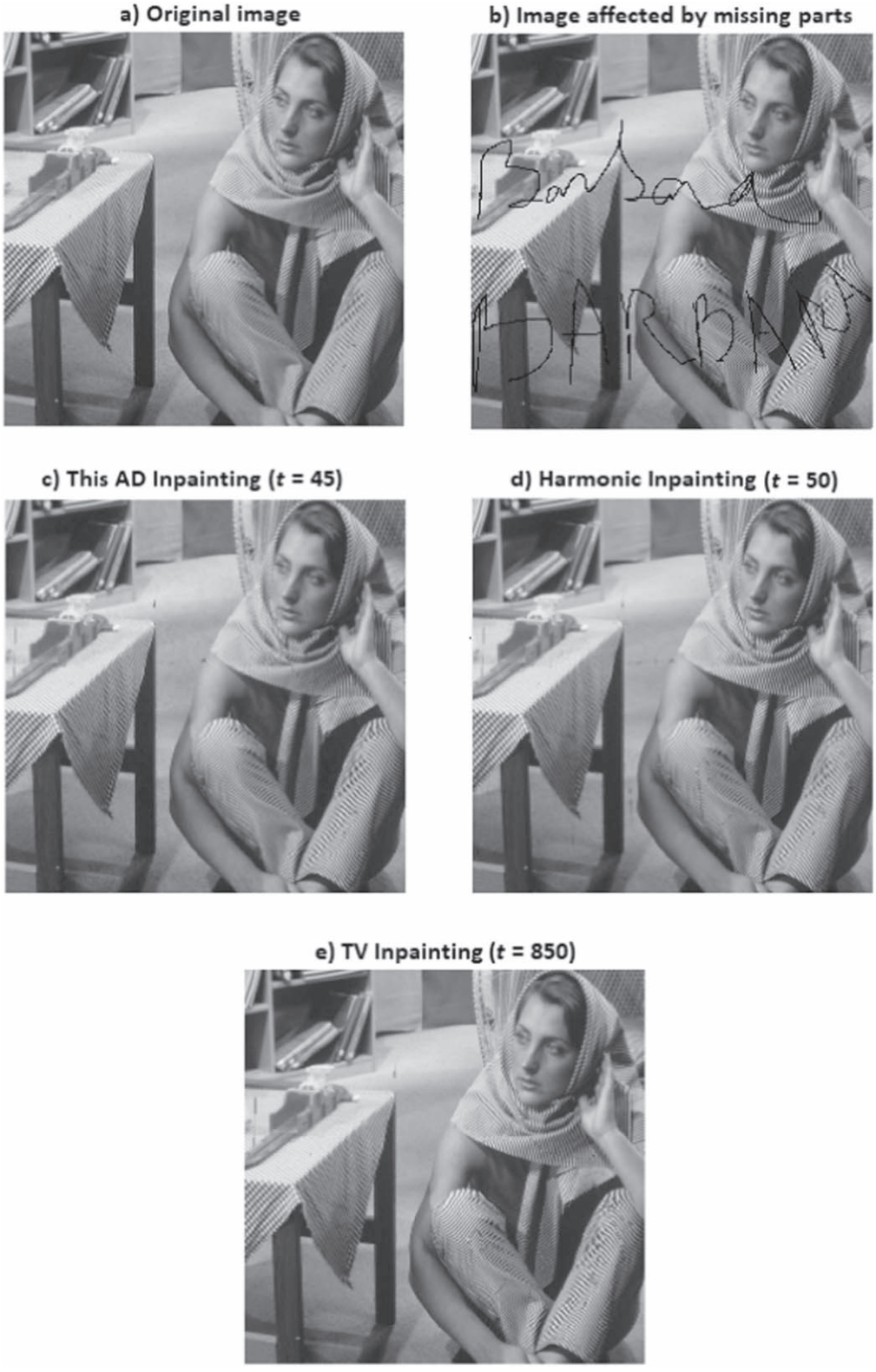

Figure 3. Image inpainted by our AD method and other schemes.

which uses an inpainting mask of the degraded image, scales that image to be inpainted to the interval $[-1, 1]$. Next, that image function u is evolved inside the inpainting domain, by applying the following CGLE:

$$\frac{\partial u}{\partial t} = \Delta u + \frac{1}{\kappa^2}(1 - \|u^2\|)u, \tag{12}$$

where $\kappa \in (0, 1)$.

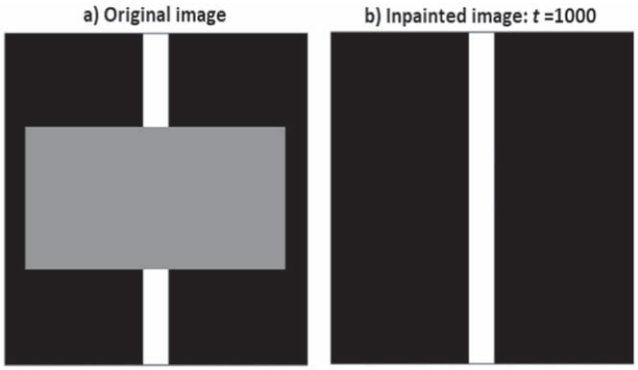

Figure 4. CGLE-based inpainting example.

Thus, the Ginzburg–Landau equation is iterated with its explicit discretization until a maximum number of iterations is reached. A finite-difference method-based iterative numerical approximation scheme is constructed for the equation (12) [24]. At each iteration of this discretization scheme only those pixels defined by the inpainting mask are updated.

A successful CGLE-based inpainting example is displayed in figure 4. The maximum number of iterations used by the inpainting algorithm is 1000 [24].

The CGLE-based inpainting algorithm provide very good interpolation results and represents a better inpainting solution than other PDE-based models [24], since it converges faster and it is much easier to implement.

4. Fluid dynamics equation-based inpainting schemes

Fluid dynamics represents the branch of physics concerned with the flow of fluids, which are specifically liquids and gases, in motion. It provides us the capability to understand the transport of mass, momentum and energy, since the foundational axioms of fluid dynamics are the conservation of mass, conservation of momentum and conservation of energy [25]. Also, fluid dynamics has a wide range of applications in many engineering domains, including the image processing areas.

Since the fluids are assumed to obey the continuum assumption, being continuous, rather than discrete, their motion can be described properly by using some PDEs for physics engineering [26]. These equations of fluid dynamics are best expressed via those conservation laws.

Thus, there exist various fluid dynamics PDEs for conservation of mass, momentum and energy. The Navier–Stokes equations represent the momentum equations for the viscous fluids [27]. Since these fluid dynamics equations describe properly the physics of numerous phenomena related to various engineering fields, they have been successfully applied in the aircraft and car design, power station design, blood flow study, magnetohydrodynamics and other areas.

The inpainting domain represents another important application area of these Navier–Stokes equations that have the important advantage of some well-developed theoretical and numerical results. Thus, an inpainting algorithm developed by Bertalmio *et al* [2, 28] uses the computational fluid dynamics related methods to propagate the isophote lines continuously into the inpanting region, from the surrounding zones.

So, the image intensity becomes the stream function for a two-dimension incompressible flow, while its Laplacian plays the role of the vorticity of the fluid. The Navier–Stokes equation-based inpainting model is characterized by the following form:

$$\frac{\partial u}{\partial t} + v \cdot \nabla w = \nu \nabla \cdot (\psi(|\nabla w|)\nabla w), \tag{13}$$

where u is the image intensity, the fluid vorticity $w = \Delta u$, the fluid velocity, representing the isophote direction, $v = \nabla^{\perp} u$, ν represents the fluid viscosity and ψ is the diffusivity function. Also, $u|_{\partial\Gamma} = u_0$, where Γ is the inpainting region.

The PDE in (13), which is a vorticity transport equation for w, transports the information automatically into the inpainting region. The fluid dynamics equation is then discretized by constructing an explicit iterative finite difference-based numerical approximation scheme [29], which is applied successfully in the inpainting experiments. The discretization algorithm has the following form:

$$w_{ij}^{n+1} = w_{ij}^{n} + \Delta t[-u^n D_x^0 w_{ij}^n - v^n D_y^0 w_{ij}^n + \nu D(\nabla \cdot (\psi(|\nabla w|)\nabla w))], \tag{14}$$

where D_x^0, D_y^0 represent the centered approximation of the first derivative and the discretization of the anisotropic diffusion component, $D(\nabla \cdot (\psi(|\nabla w|)\nabla w))$, can be performed, by applying the finite differences [29], as in the approximation schemes of the previously described nonlinear diffusion-based inpainting models (see the equations [8, 10]).

The inpainting algorithm based on these fluid dynamics equations provides a very good reconstruction of the damaged image [28, 30]. Thus, it produces sharp results and overcomes the image blurring, the color artifacts and other unintended effects.

An example of image interpolation performed using the Navier–Stokes equations is provided in figure 5. A text removal process is described in that figure. The text is removed from the image in (a) (courtesy of Konstantinos Papafitsoros [31]) by applying the described inpainting solution and using the inpainting mask displayed in (b), after 100 iterations of the numerical scheme (14), the interpolation output being provided in (c).

5. CDD inpainting

Another important category of PDEs of engineering physics that are very useful for the structural inpainting domain are the CDD equations, which uses the thermal diffusion principle in physics. Thus, CDD inpainting proposed by Chan and Shen [32], represents a nonlinear third-order PDE-based structural image interpolation model that is constructed as a solution to improve the TV inpainting scheme given by (3).

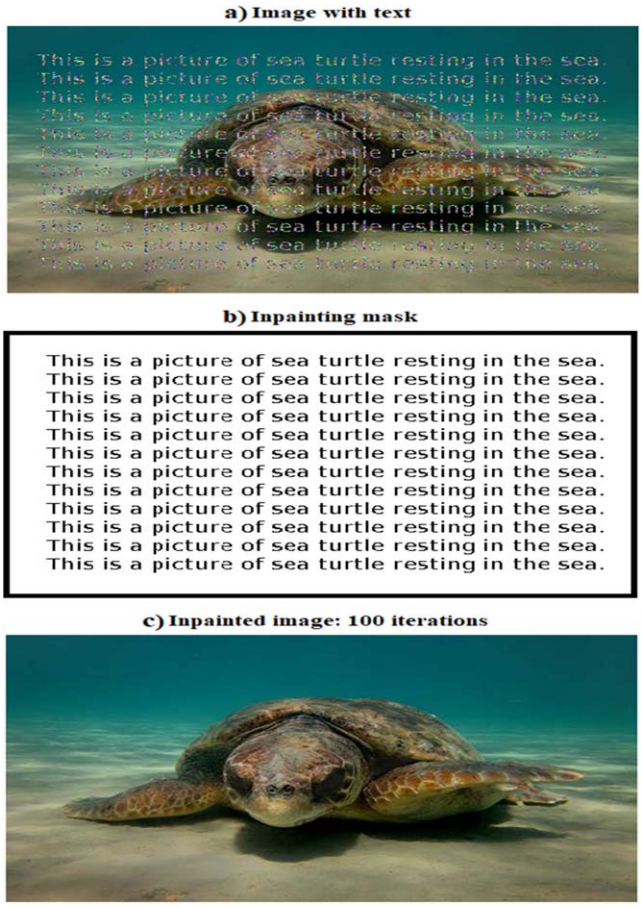

Figure 5. Navier–Stokes equation-based inpainting example.

Figure 6. CDD inpainting-based text removal example.

This CDD inpainting model is based on the curvature information of the isophotes. It is characterized by the next PDE:

$$\begin{cases} \dfrac{\partial u}{\partial t} = \nabla \cdot \left(\dfrac{g(\kappa)}{|\nabla u|} \nabla u \right) - \lambda_{\Gamma}(u - u_0), \\ u(0, x, y) = u_0 \end{cases} \tag{15}$$

where the curvature of the isophote $\kappa = \nabla \cdot \left[\frac{\nabla u}{|\,[\nabla u]\,|} \right]$, the diffusivity function $g(s) = s^p,\ p \geqslant 1$ and Γ is the inpainting region [2, 32, 33].

The CDD-based equation in (15) diffuses the smoothness perpendicularly to the level lines. It preserves the direction of these isophotes and it is able to connect them across large distances. This better connectivity makes CDD inpainting model a better interpolation solution than TV inpainting and other second-order PDE inpainting schemes.

The CDD inpainting model is solved numerically by applying a numerical approximation algorithm constructed using the finite difference method [32]. The flux of this CDD-based model is computed from (15) as:

$$j = -\frac{g(\kappa)}{|\nabla u|} \nabla u. \tag{16}$$

Therefore, the CDD equation in (15) becomes $\frac{\partial u}{\partial t} = -\nabla \cdot j$ [2, 32]. So, it is then discretized by using the next iterative explicit numerical approximation scheme:

$$u^{n+1} = u^n - \Delta t [\nabla \cdot j]^{(n)}, \tag{17}$$

where $t = n\Delta t$ and $[\nabla \cdot j]^{(n)}$ represents the approximation of the divergence $\nabla \cdot j$, which is determined by using the half-point central differences for the divergence operator [32].

The iterative numerical approximation algorithm (17) is converging stable to the image representing the final reconstruction result [32]. It has been successfully applied in the inpainting experiments. CDD inpainting provides very good image interpolation results, performing properly a lot of inpainting tasks, such as the disocclusions, recovery of the old photos corrupted by scratches, text and object removal from images [32, 33].

Such a CDD inpainting based text removal example is displayed in the next figure [32, 33]. The text from the image depicted in figure 6(a) is removed using the inpainting mask described in (b), the text removal output being displayed in (c).

However, the CDD-based inpainting framework has some disadvantages. One of these drawbacks is its noise sensitive character, since the CCD inpainting model is not performing properly in noisy image conditions [2, 31].

6. Cahn–Hilliard equation-based inpainting solutions

In physical sciences, in the process of phase separation, two components of a binary fluid spontaneously separate and form domains pure in each component. This process is described by a PDE of mathematical physics, which is the Cahn–Hilliard equation [34].

This equation originating in material science for modeling phase separation and phase coarsening in binary alloys has the following form:

$$\frac{\partial c}{\partial t} = D\nabla^2(c^3 - c - \gamma\Delta c), \tag{18}$$

where c represents the fluid's concentration and D is the diffusion coefficient.

This nonlinear fourth-order PDE from the material science could be also used in the structure-based inpainting domain, but in a modified version that contains a fidelity term that is added to it [2, 35, 36]. Thus, the Cahn–Hilliard inpainting model is based on the following modified Cahn–Hilliard equation and some Neumann boundary conditions:

$$\begin{cases} u_t = -\Delta\left(\varepsilon\Delta u - \frac{1}{\varepsilon}W'^{(u)}\right) - \lambda(x, y)(u - u_0), \text{ in } \Omega \\ \frac{\partial u}{\partial \nu} = \frac{\partial \Delta u}{\partial \nu} = 0, \text{ on } \partial\Omega \end{cases}, \tag{19}$$

where the nonlinear double-well potential function $W(u) = u^2(u-1)^2$ and $\lambda(x, y) = \begin{cases} \lambda_0 \geqslant 1, (x, y) \in \Omega\backslash\Gamma \\ 0, (x, y) \in \Gamma \end{cases}$, Γ being the inpainting region. The observed image that is affected by missing regions and needs to be inpainted is $u_0 \in L^2(\Omega)$.

The nonlinear fourth-order PDE-based model (19) is well-posed, the global existence of a unique and weak solution of it being proved in [35]. The solution is numerically computed by applying a consistent, fast converging and stable numerical approximation algorithm, which is the *convexity splitting* fast solver [35].

This convexity splitting technique divides the energy functional of the PDE into two components: the convex energy and the concave one. Next, the component of the Euler–Lagrange equation obtained from the convex part is treated implicitly, while the component derived from the concave part is treated explicitly in the numerical approximation [35, 36]. A time-stepping scheme results for these splittings [36], which is finally translated to the following numerical approximation scheme:

$$\frac{u_{n+1} - u_n}{\Delta t} + \varepsilon\Delta\Delta u_{n+1} - C_1\Delta u_{n+1} + C_2\Delta u_{n+1} = \frac{1}{\varepsilon}\Delta W'(u_n) - C_1\Delta u_n + \lambda(u_0 - u_n) + C_2 u_n, \tag{20}$$

where $C_1 > \frac{1}{\varepsilon}$ and $C_2 > \lambda_0$.

Cahn–Hilliard inpainting provides an effective image reconstruction that outperforms the state of the art nonlinear second and third order PDE-based approaches. It inpaints the degraded image by producing a smooth continuation of the level lines (isophotes) into the inpainting domain Γ. Therefore, while the Cahn–Hilliard inpainting technique is operating somewhat similarly to the curvature driven diffusion-based algorithms, it converges faster than CDD inpainting [35].

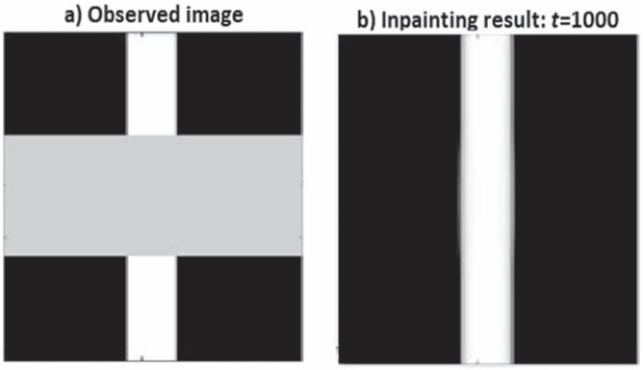

Figure 7. Cahn–Hilliard inpainting example.

A Cahn–Hilliard inpainting example is provided in figure 7. One can see the observed image containing the inpainting region in (a), while the interpolation result achieved after 1000 iterations of the Cahn–Hilliard inpainting scheme is displayed in (b).

Some image interpolation frameworks that improve this Cahn–Hilliard inpainting model have been also developed in the recent years. Thus, a grayscale image interpolation technique based on a generalized complex version of the Cahn–Hilliard equation is proposed in [37]. A rigorous mathematical treatment, studying the well-posedness of the model, is also performed.

Other versions of Cahn–Hilliard inpainting can be achieved by considering other forms for the potential function $W(u)$. Thus, it was developed a Cahn–Hilliard inpainting model with a non-smooth logarithmic potential in [38].

Another improved version is the Cahn–Hilliard inpainting scheme with the non-smooth double obstacle potential [39, 40], which is based on the following form of the potential function:

$$W(s) = \hat{\beta}(s) + \frac{1}{2}(1 - s^2), \tag{21}$$

where the $\hat{\beta}$ represents the indicator function of the interval $[-1, 1]$, taking zero value in this interval and the value $+\infty$ otherwise.

Cahn–Hilliard inpainting model using the double obstacle potential outperforms Cahn–Hilliard inpainting based on classical smooth quartic double well potential function. A method comparison example illustrating this fact is displayed in figure 8.

One can see in the figure that Cahn–Hilliard inpainting with non-smooth potential achieves better reconstruction results (c) than Cahn–Hilliard inpainting scheme using the double well potential (d). A mathematical analysis that

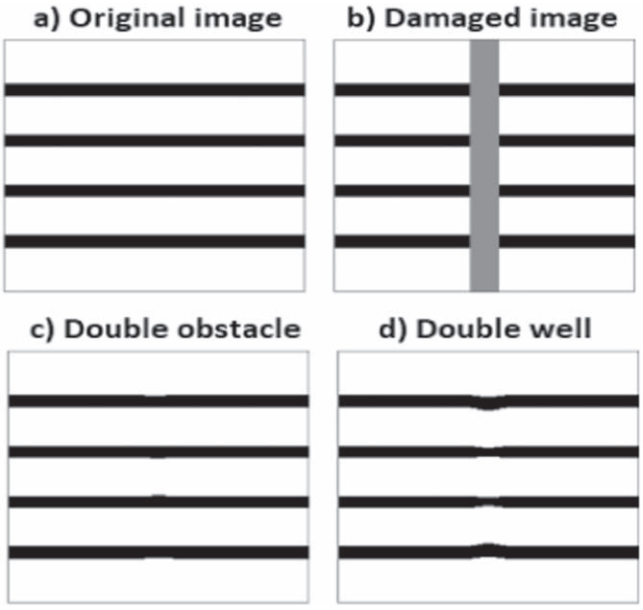

Figure 8. Method comparison: Cahn–Hilliard inpainting versions.

investigates the existence of Cahn–Hilliard equations' solutions is also performed in [39].

An extension of the Cahn–Hilliard inpainting scheme, which represents a generalization of it for the gray-value images of bounded variation, is the TV–H^{-1} inpainting model [2, 35, 41]. Thus, the TV–H^{-1} inpainted image u of $u_0 \in L^2(\Omega)$ represents the stationary solution of the next equation:

$$\frac{\partial u}{\partial t} = \Delta p + \lambda(x, y)(u_0 - u),\ p \in \partial \mathrm{TV}_\infty(u), \qquad (22)$$

where $\partial \mathrm{TV}_\infty(u)$ represents the sub-differential of $\mathrm{TV}_\infty(u) = \begin{cases} |Du|(\Omega), \text{ if} |u| \leqslant 1 \text{a.e.in } \Omega \\ +\infty, \text{ otherwise} \end{cases}$ and $|Du|(\Omega)$ is the TV of u [35].

The stationary solution of the PDE in (22), $u \in BV(\Omega)$, is determined by applying a time-stepping numerical approximation algorithm that is similar to the previous one, described in (20). Like Cahn–Hilliard inpainting, this fourth-order PDE interpolation approach derived from it provides very good reconstruction results, outperforming the TV inpainting, but after hundreds of iterations of the numerical scheme.

7. Conclusions

An overview of the most important PDEs that describe physical phenomena and are succesfully applied in the structure-based inpainting domain has been provided in this work. Thus, we have considered several classes of PDEs for engineering physics and described the state of the art image interpolation frameworks related to them.

So, structural inpainting models based on anisotropic diffusion, reaction diffusion, CDD, fluid dynamics and phase separation are disscused in this research paper. While the described nonlinear diffusion completion models are based on second-order PDEs, the inpainting approaches related to the other physical phenomena are based on PDEs of higher-order. Thus, we have addressed some third-order PDE-based interpolation models, such as CDD inpainting or those using Navier–Stokes equations, and fourth-order PDE reconstruction schemes, such as the inpainting solutions based on the various versions of the modified Cahn–Hilliard equation.

The largest section of this survey is dedicated to the nonlinear second-order diffusion-based structural inpainting models, which can be expressed in variational or PDE form. Besides the state of the art variational and non-variational PDE-based interpolation techniques, we have described here our own contributions in this inpainting field.

The other sections do not contains our contributions in those areas, since we have not conducted much research in those directions. The structural inpainting methods developed by us provide effective reconstruction results, work succesfully in noisy conditions and also they overcome the unintended effects.

They outperform numerous state of the art structure-based interpolation techniques, but, unfortunately, they do not work properly for textured images. Developing some reconstruction approaches that are able to inpaint both textured and non-textured images will constitute the focus of our future research in this image processing domain.

ORCID iDs

Tudor Barbu https://orcid.org/0000-0002-9919-7776

References

[1] Stone M and Goldbart P 2009 *Mathematics for Physics I* (London: Pimander-Casaubon)
[2] Schonlieb C B 2015 *Partial Differential Equation Methods for Image Inpainting* vol 29 (Cambridge: Cambridge University Press)
[3] Igehy H and Pereira L 1997 Image replacement through texture synthesis *Int. Conf. on Image Processing* vol 3, pp 186–9
[4] Criminisi A, Perez P and Toyama K 2004 Region filling and object removal by exemplar-based image inpainting *IEEE Trans. Image Process.* **13** 1200–12
[5] Mehrer H 2007 *Diffusion in Solids–Fundamentals, Methods, Materials, Diffusion controlled Processes* (Berlin: Springer)
[6] Song B 2003 *Topics in Variational PDE Image Segmentation, Inpainting and Denoising* (Berkeley, CA: University of California Press)
[7] Hazawinkel M 2001 *Variational Calculus* (*Encyclopedia of Mathematics*) (Berlin: Springer)
[8] Ambrosio L and Tortorelli V 1990 Approximation of functionals depending on jumps by elliptic functionals via Γ-convergence *Commun. Pure Appl. Math.* **43** 999–1036
[9] Chan T and Shen J 2001 Morphologically invariant PDE inpaintings *UCLA CAM Report* University of Minnesota Digital Conservancy 1–15 IMA Preprints Series
[10] Papafitsoros K, Schonlieb C B and Sengul B 2013 Combined first and second order total variation inpainting using split Bregman *Image Process. On Line* **2013** 112–36

[11] Bredies K and Holler M 2015 A TGV-based framework for variational image decompression, zooming, and reconstruction: I. Analytics *SIAM J. Imaging Sci.* **8** 2814–50
[12] Afonso M V and Sanches J M R 2015 Blind Inpainting Using l_0 and Total Variation Regularization *IEEE Trans. Image Process.* **24** 2239–53
[13] Neri M and Zara E R 2014 Total variation-based image inpainting and denoising using a primal-dual active set method *Philippine Sci. Lett.* **7** 97–103
[14] Chan T F, Kang S H and Shen J 2002 Euler's elastica and curvature based inpaintings *SIAM J. Appl. Math.* **63** 564–92
[15] Barbu T 2016 Variational image inpainting technique based on nonlinear second-order diffusions *Comput. Electr. Eng.* **54** 345–53
[16] Barbu T 2017 Hybrid image interpolation technique based on nonlinear second and fourth-order diffusions *13th Int. Symp. on Signals, Circuits and Systems, ISSCS'* 17 (IEEE) 1–5
[17] Weickert J 1998 *Anisotropic Diffusion in Image Processing* (*European Consortium for Mathematics in Industry*) (Stuttgart: B. G. Teubner)
[18] Barbu T and Munteanu I 2017 A well-posed second-order anisotropic diffusion-based structural inpainting scheme *ROMAI J., ROMAI Soc.* **13** 1–9
[19] Barbu T 2017 Structural image interpolation using a nonlinear second-order hyperbolic pde-based model *6th IEEE Int. Conf. on e-Health and Bioengineering, EHB 2017 (Sinaia, Romania, June 22-24)* (IEEE) 5–8
[20] Barbu T 2018 Second-order anisotropic diffusion-based framework for structural inpainting *Proc. Rom. Acad.* A **19** 329–36
[21] Kuttler C 2011 *Reaction-Diffusion Equations with Applications* (Sommersemester)
[22] Chen Y, Yu W and Pock T 2015 On learning optimized reaction diffusion processes for effective image restoration *Proc. IEEE Conf. Comput. Vis. Pattern Recognit* pp 5261–9
[23] Yu W, Heber S and Pock T 2015 Learning reaction-diffusion models for image inpainting *Pattern Recognition. DAGM 2015* (*Lecture Notes in Computer Science) (Ed.),*) ed J Gall *et al* vol 9358 (Cham: Springer)
[24] Nakano S 2010 Image inpainting with the complex Ginzburg–Landau Equation *Dissertation* Science: Department of Mathematics
[25] Acheson D J 1990 *Elementary Fluid Dynamics* (Oxford: Clarendon)
[26] Anderson J D 2009 Governing equations of fluid dynamics *Computational Fluid Dynamics* 2 3rd edn (Heidelberg: Springer)
[27] Temam R 1984 *Navier–Stokes Equations: Theory and Numerical Analysis* (Providence, RI, US: ACM Chelsea Publishing)
[28] Bertalmio M, Bertozzi A L and Sapiro G 2001 Navier–Stokes, fluid dynamics, and image and video inpainting *IEEE Computer Society Conference on Computer Vision and Pattern Recognition. CVPR 2001 (Kauai, Hawaii, US, December 8-14)* (IEEE) pp 355–620-7695-1272-0
[29] Johnson P 2008 *Finite Difference for PDEs* (School of Mathematics, University of Manchester) Semester I
[30] Au W and Takei R 2002 Image Inpainting with the Navier–Stokes Equations Final Report, APMA 930
[31] Papafitsoros K 2015 *Novel higher order regularisation methods for image reconstruction (Doctoral thesis)* University of Cambridge
[32] Chan T F and Shen J 2001 Non-texture inpainting by curvature-driven diffusions (CDD) *J. Visual Commun. Image Rep.* **4** 436–49
[33] Chan T F and Shen J 2005 *Image Processing and Analysis: Variational, PDE, Wavelet, and Stochastic Methods* 94 (Philadelphia, PA: SIAM)
[34] Cahn J W and Hilliard J E 1958 Free energy of a nonuniform system: I. Interfacial free energy *J. Chem. Phys.* **28** 258
[35] Burger M and He L 2009 Cahn–Hilliard inpainting and a generalization for grayvalue images *SIAM J. Imaging Sci.* **2** 1129–67
[36] Gillette 2006 A image inpainting using a modified Cahn–Hilliard equation *PhD Thesis* University of California, Los Angeles, CA
[37] Cherfils L, Fakih H and Miranville A 2017 A complex version of the Cahn–Hilliard equation for grayscale image inpainting *Multiscale Model. Simul.* **15** 575–605
[38] Cherfils L, Miranville A and Zelik S 2011 The Cahn–Hilliard equation with logarithmic potentials *Milan J. Math.* **79** 561–96
[39] Garcke H, Lam K F, Sitka E and Styles V 2018 Cahn–Hilliard inpainting with the double obstacle potential *SIAM J. Imaging Sci.* **11** 2064–89
[40] Bosch J, Kay D, Stoll M and Wathen A J 2014 Fast solvers for Cahn–Hilliard inpainting *SIAM J. Imaging Sci.* **7** 67–97
[41] Osher S, Sole A and Vese L 2003 Image decomposition and restoration using total variation minimization and the H^{-1} norm *Multiscale Model. Simul.: A SIAM Interdiscip. J.* **1** 349–70